7.1 Introduction

In general the structural phase transitions in a crystalline material are clearly noticeable with change in lattice symmetry as a function of temperature (T), composition (x), or pressure (P). Generally, a symmetry element of high symmetry phase is lost at the phase transition temperature (T_C), and transformed into a structure having lower symmetry. The structural phase transitions involving change of space group symmetry are ubiquitous in nature, there are known examples of less commonly observed isostructural phase transitions which preserve the space group symmetry and the type of occupied Wyckoff positions. Such transitions manifest through sharp change of some macroscopic property of the system like volume, resistivity, etc. [Scott (2010)].

This transition is accompanied with an anomaly in the dielectric constant, dc conductivity, and proton-resonance spectra without breaking the internal symmetry. In the case of antiferromagnetic inorganic compounds, the deformation in the arrangement of magnetic atoms existing above the Neel temperature (T_N) is a natural consequence of the arrangement of adjacent magnetic atoms in antiparallel spin orientation below the transition temperature. This deformation in the crystal structure of antiferromagnetic compounds on passing through the magnetic transition temperature was investigated in the pioneering work in the early 1950s by Greenwald et al. (1951). Recently, isostructural phase transitions occurring across antiferromagnetic transition in multiferroics have been shown to be responsible for the magnetoelectric coupling [Lee et al. (2008), Singh et al. (2008), Bhattachrjee et al.(2011)].

While there has been considerable progress in the understanding of the magnetoelectric coupling and magnetic structure of $BiFeO_3$, the stability field of its room temperature phases and the sequence of the structural phase transitions it undergoes as a function of

temperature continue to remain controversial and has long history too, as discussed in resent literature [Arnold et al. (2009), Kornev et al. (2009), Palai et al. (2008), Haumont et al (2008), Selbach et al. (2008), Kornev et al. (2007)]. There is unanimity on the room temperature structure of α-phase of $BiFeO_3$ that is rhombohedrally distorted pervskite structure in R3c space group [Glazer (1972) and (1975)].

Selbach et al. (2008) predicated two ferroelectric phase transitions (cubic→rhombohedral R3c) of $BiFeO_3$ at T_N, and a continuous volume expansion occurs across the second order anti-ferromagnetic transition at 643 K. [Kothai et al. (2013)] have reported using x-ray and neutron powder diffraction study BF-xPT compositions close to the morphotropic phase boundary reveals two type of structural phase transition. One, cooling from cubic>tetragonal(T2)+tetragonal(T1)>tetragonal(T1) and another one is cubic> Tetragonal(T2)+tetragonal(T1)+rhombohedral(R3c)>tetragonal(T1)+rhombohedra (R3c).

In pure $BiFeO_3$, the temperatures corresponding to the α to β and the β to γ transitions lie above 1093 K [Palai et al (2008)], at which BiFeO3 is no longer chemically stable and tends to decompose into $Bi2Fe_4O_9$ and $Bi_{25}FeO_{39}$ phases [Selbach et al. (2009)] followed by melting at still higher temperatures.

[Ranjan et al.(2010)] have also shown that BF-xPT , which exhibiting giant tetragonality of about 19% does not follow the direct cubic to tetragonal transition. The cubic phase transforms to two intermediate coexisting phases like (major) tetragonal with space group P4mm and (minor) monoclinic phase with space group Pm. This intermediate tetragonal phase gradually disappears and monoclinic phase, which is pseudotetragonal in nature, transforms itself to a tetragonal phase with giant tetragonality upon cooling.

In this chapter, we present the results of a high temperature synchrotron x-ray diffraction (SXRD) study of different sizes of BF-0.5PT

7.2 Experimental details

The different sizes of samples of BF-0.5PT are synthesized by sol-gel process, the details of which have been described in chapter II. The high temperature SXRD measurements of 31nm, 45nm and bulk samples of BF-0.5PT were carried out at a wave length of 0.7783 Å in the 300 to 1000 K range at the BL02B2 beam line of Spring- 8, Japan using a large Debye-Scherrer camera equipped with an imaging plate as a two-dimensional detector. The temperature of the sample was varied using a hot N_2 gas-flow system with an accuracy of ± 1 K.

The SXRD data were analyzed by both Lebail and Rietveld techniques, using FULLPROF (Carvajal (2008)) package.

7.3 Results and Discussion

7.3.1 Evolution of the SXRD profile of BF0.5PT powder of different sizes with temperature.

The evolution of 100, 110 and 200 pseudocubic peaks from room temperature to 1000K was shown in fig.7.1 and fig. 7.2 for 31nm and 45nm respectively. As we discussed in chapter III, that BF-0.50PT samples of these sizes contains two tetragonal phase with different tetragonality. Both (100)pc and (110)pc peak are doublet at room temperature for 31nm and 45 nm powders which primarily signature of tetragonal phase. The splitting are persists up to 725K for 31 nm powder whereas for 45 nm powder it is up to 900K, after which all peaks become singlet. On the other hand, (002) peak which is broad hump is shifting towards higher angle with increasing temperature. The broadening of the peak suggests coexistence of two phases which confirmed by Reitveld refinement of nano BF-

0.5PT powder at room temperature as discussed in chapter-III. The disappearance of broadening was observed from the figure, at around 800K and 900K for 31 nm 45 nm size powder respectively. This suggests that there some structural transition on that particular temperature, which is matter of investigation. This is further discussed in next section of this chapter. The fig.7.3 shows temperature dependent synchrotron x-ray diffraction pattern for bulk BF-0.5PT sample of size 110nm. Both (100)pc and (110)pc are sharp and well splitted, which confirm that this sample is more crystalline that 31nm and 45nm. The sharp (002) peak which shifting towards higher 2θ with temperature was disappears at 900K. The SXRD data was collected from 600K to 1000K in interval of 100K. So due to less data, it is very difficult to predict the exact transition temperature. But it believes that Bhattacharjee et al. already have discussed the high temperature XRD of bulk sample of BF-0.4PT, which was prepared through solid state route [Bhattacharjee et al. (2011)]. Since BF-0.4PT powder has tetragonal structure and our sample is close to this composition so, its transition temperature is close to it. So we did not take so much data to re-establish the result. Although there is small broadening occurs at 700K and 800K in (002) peak, this may be some phase transition in sample which may discussed latter in this chapter.

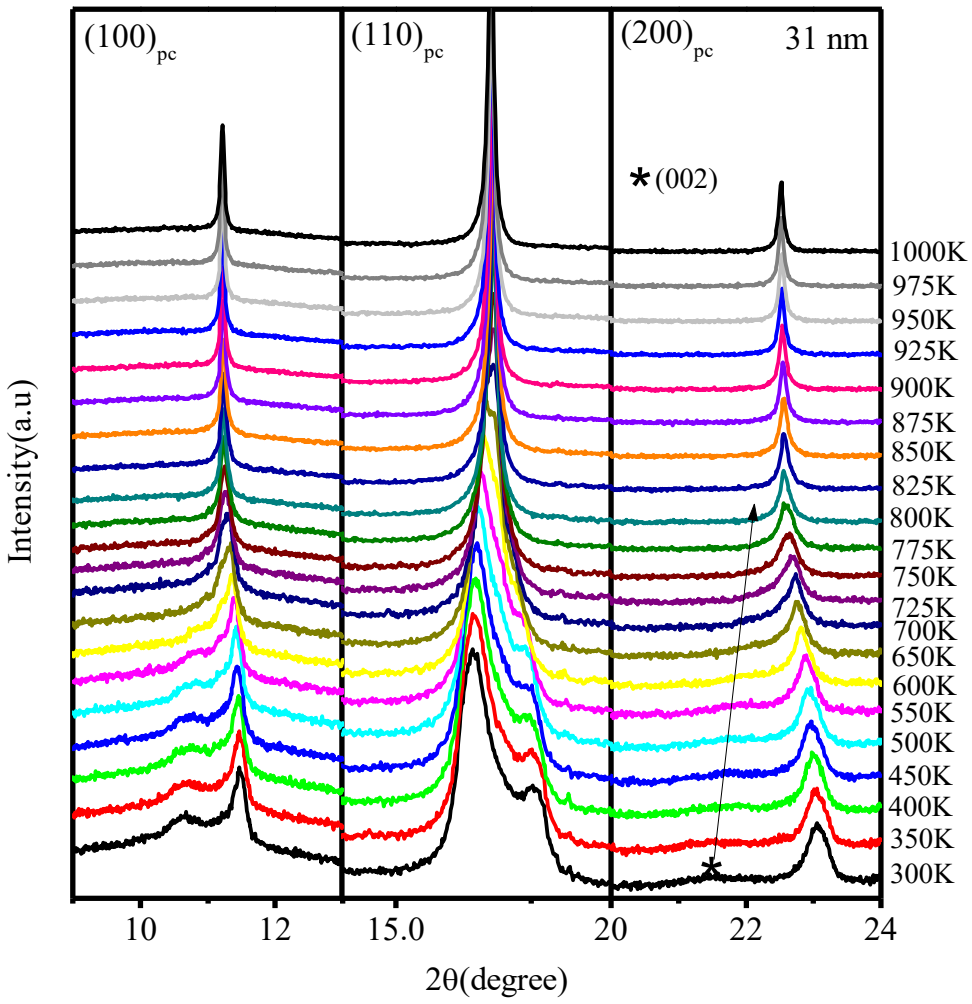

Fig. 7.1 Evolution of SXRD profile of (100)pc,(110)pc and (200)pc reflections of 31 nm BF-0.50PT with temperature showing structural phase transition.

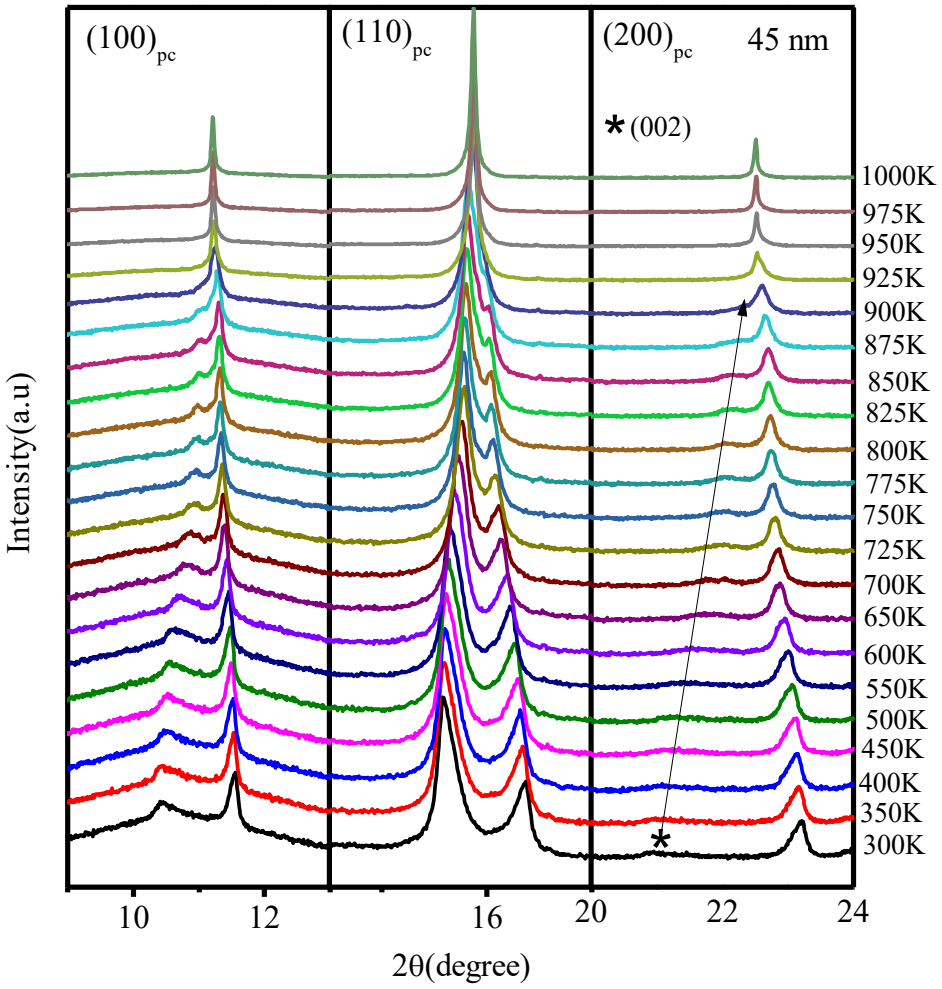

Fig. 7.2 Evolution of SXRD profile of (100)pc,(110)pc and (200)pc reflections of 45 nm BF-0.50PT with temperature showing structural phase transition.

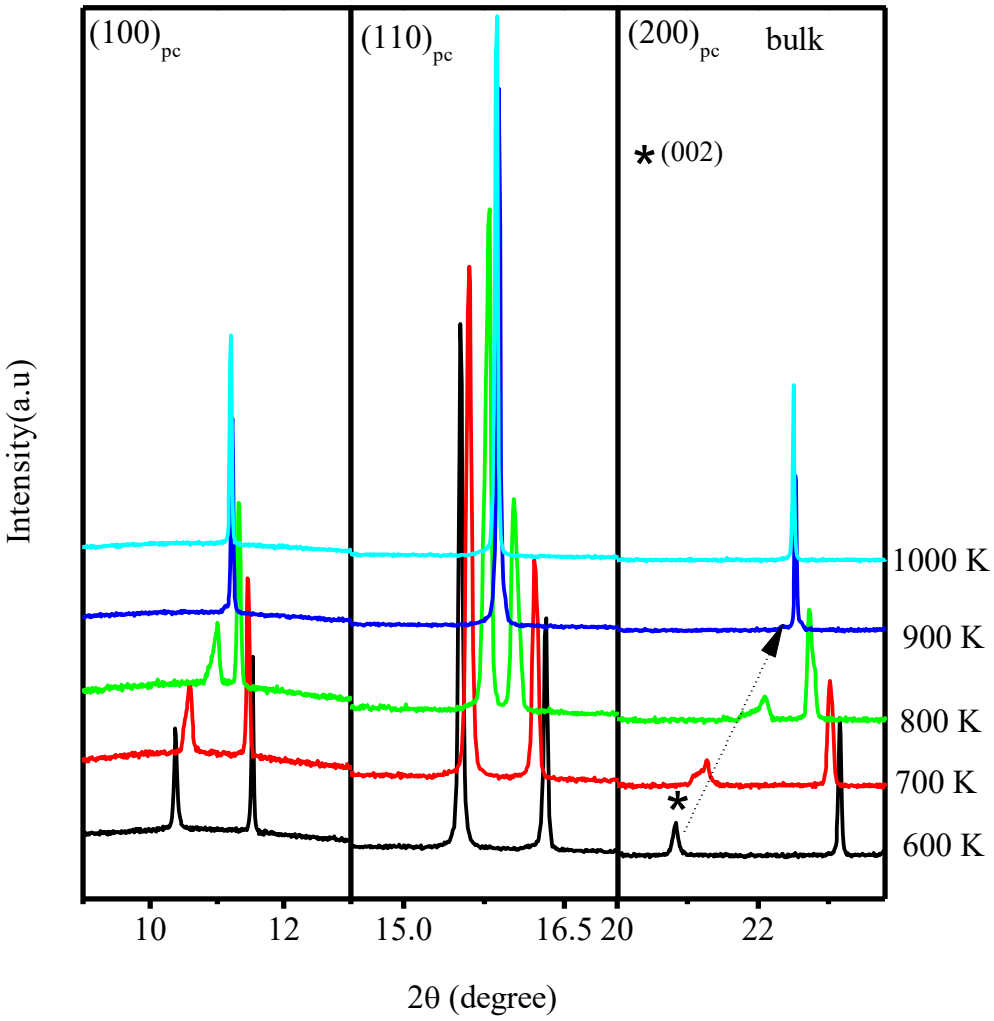

Fig. 7.3 Evolution of SXRD profile of (100)pc,(110)pc and (200)pc reflections of bulk BF-0.50PT with temperature showing structural phase transition.

7.3.2 Temperature dependent profile refinement of BF-0.5PT of different sizes

The LeBail refinement was carried out for all the samples using FULLPROF package [Carvajal (2008]. In these refinements, pseudo-voigt function and linear interpolation function were used to define the profile shape and background respectively. The observed and calculated profiles show excellent fit for all the samples, as can be seen from the

difference (bottom line) profile given in fig. 7.4. This confirms that sample of size 31 nm having coexistence two tetragonal phases at room temperature. The 31 nm powders consist two tetragonal phases blow 750K, which upon heating to higher temperature lower tetragonal phase become cubic phase. Further, the (200)pc peak is much broader than nearby (220)pc peak at room temperature. The bradening of peak decreases as temperature increases. This broadening indicates the coexistence of more than one phase in sample. The (111)pc peak remain a singlet and there is no effect of temperature on it. We therefore conclude that the tetragonal phase for powder of 31 nm transforms into two cubic phases at 800K.Fig. 7.5 shows that sample of size 45 nm having also coexistence two tetragonal phases at room temperature. These two tetragonal phases with different tetragonality persist blow 900K, which upon heating to higher temperature lower tetragonal phase become cubic phase. Further, the (200)pc peak is much broader than nearby (220)pc peak at room temperature. The broadening of peak decreases as temperature increases. There is no any effect on (111)pc peak, it remains a singlet even after increasing temperature. We therefore conclude that the tetragonal phase for powder of 45 nm transforms into two cubic phases at 950K. Fig. 7.6 shows that bulk powder having single tetragonal phases at 600K. It is already discussed in chapter III that at room temperature it contains single tetragonal phase. So there is no any structural phase transition observe upto the 600K. At 800K the tetragonal phase (T1) of size 110 nm undergoes a first-order isostructural phase transition to another tetragonal phase (T2) with lower tetragonality without losing the P4mm space group symmetry, which earlier reported by [Bhattacharjee et al. (2011)] in this type of system. For bulk powder it is very difficult to find exact temperature at which it transform into cubic, because we have very less data points to estimate it. But we can say that it is lies in between 900K to 1000K.

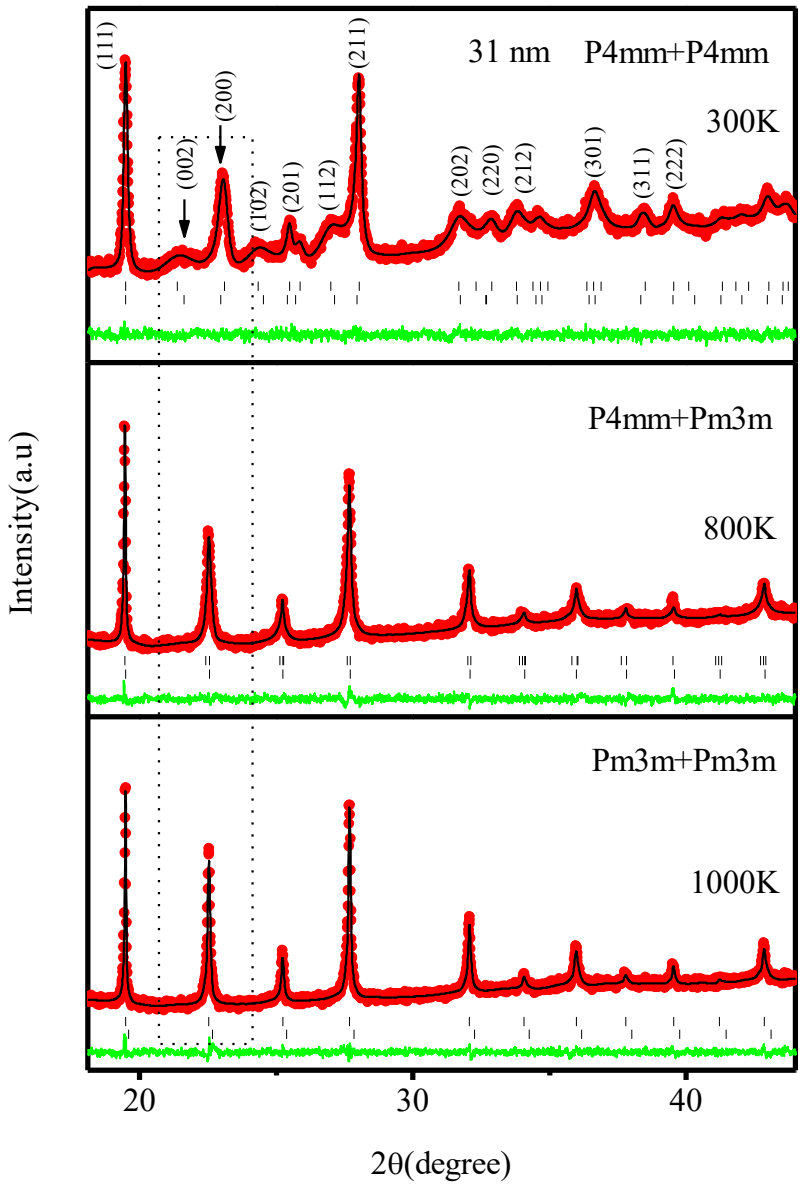

Fig. 7.4 LeBail refinement plot of three different best possible structural models at 300K, 800K and 1000K. The vertical tick marks above the difference profile correspond to the positions of the Braggs reflections.

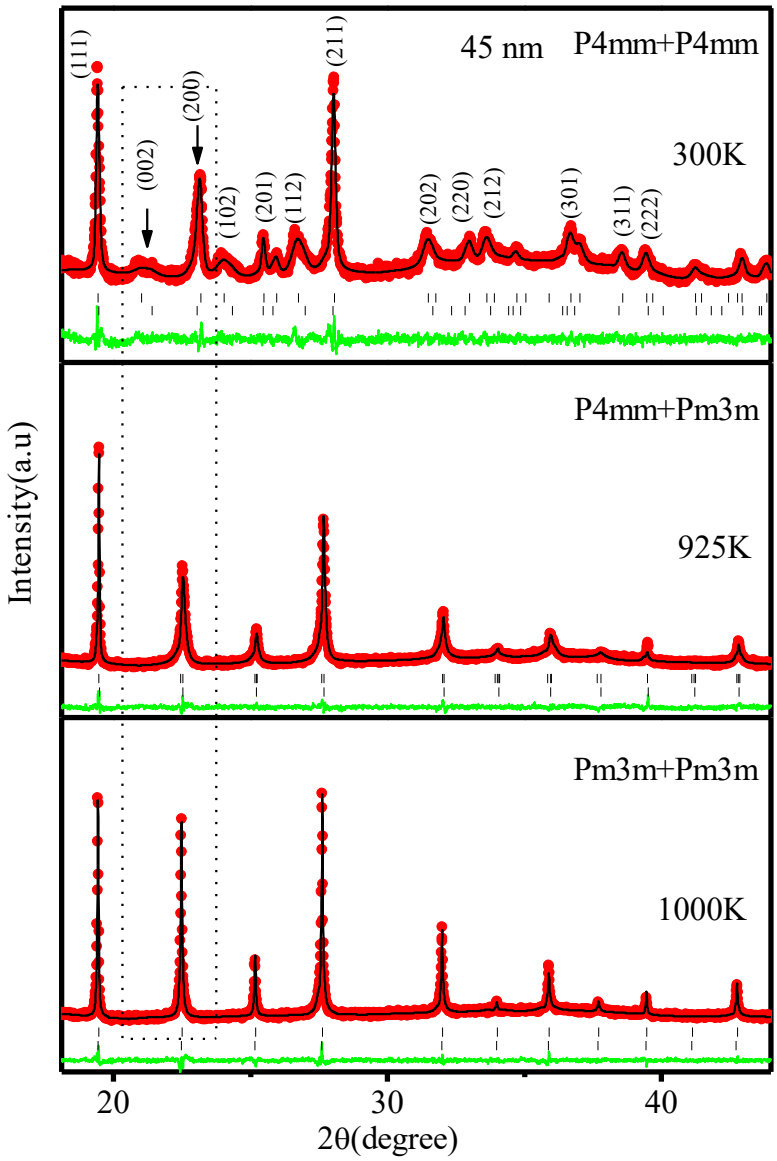

Fig. 7.5 LeBail refinement plot of three different best possible structural models at 300K, 925K and 1000K. The vertical tick marks above the difference profile correspond to the positions of the Braggs reflections.

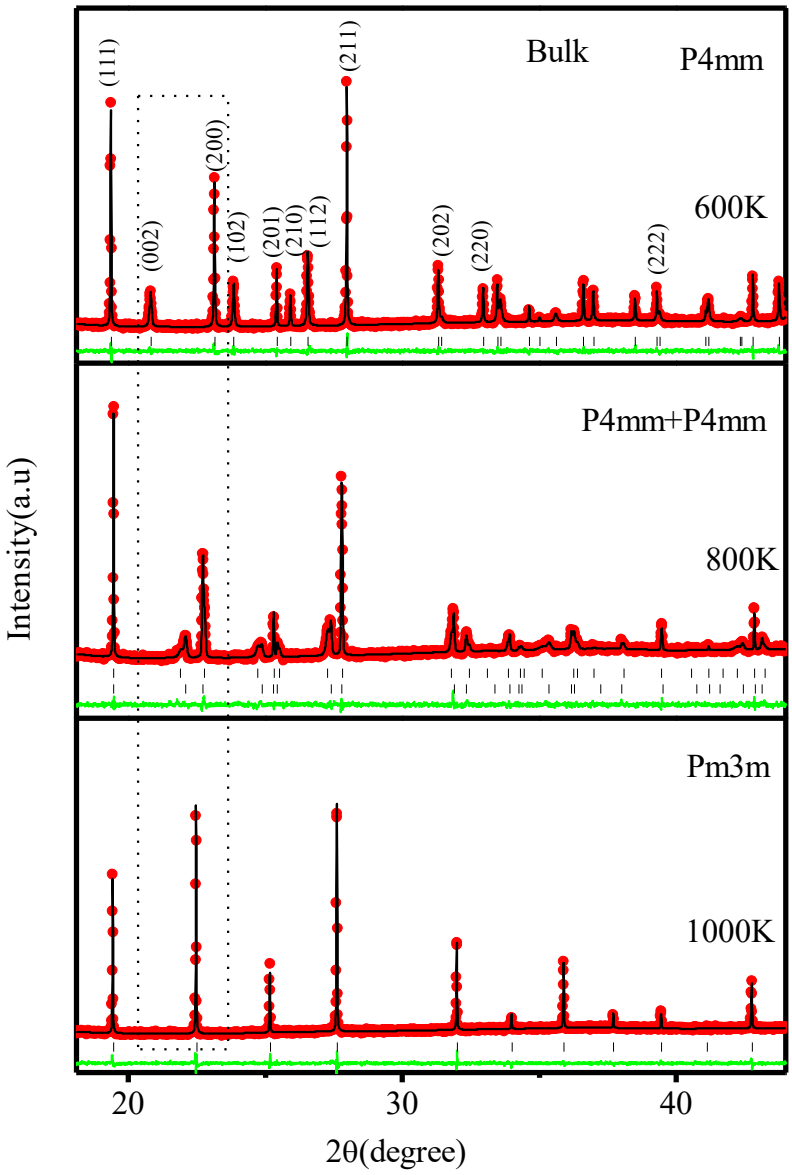

Fig. 7.6 LeBail refinement plot of three different best possible structural models at 600K, 800K and 1000 K. The vertical tick marks above the difference profile correspond to the positions of the Braggs reflections.

For reliability of determining the tetragonal to cubic phase transition temperature, we plot full width half maximum (FWHM) of the (200)pc peak as a function of temperature for all the sizes. The values of FWHM were obtained by least square fitting of (200) reflection. In fig. 7.7 indicates that for 31 nm BF-0.5PT powder value of FWHM increase up to 725K and then decreasing continuously up to 1000K. The change in slop indicates phase transition in sample at that particular temperature. In first part of fig. 7.7 and fig. 7.8, it is clearly shows that two tetragonal phase with different tetragonality are existing. In second part of figure, the tetragonal phase with lower tetragonality is converting into cubic phase and this phenomenon is repeating into third part of figure where another tetragonal phase is converting into cubic phase.

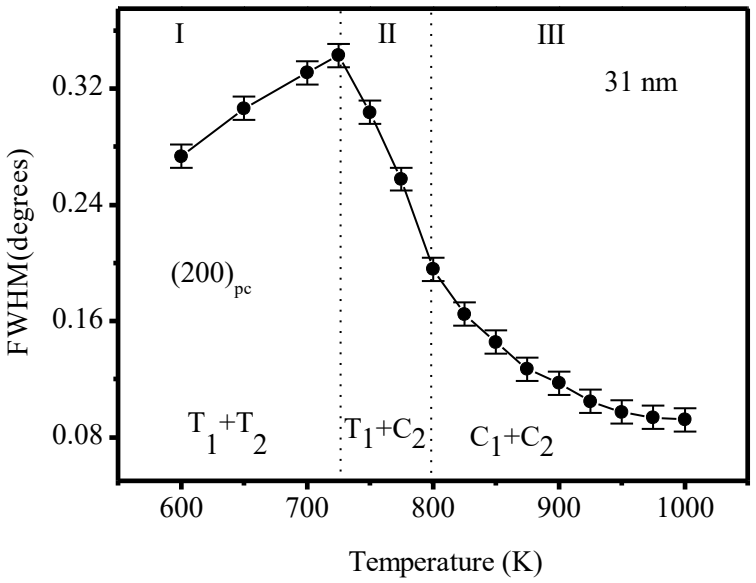

Fig. 7.7 The variation of FWHM of the (200)pc reflection of 31 nm size of BF-0.5PT powder with temperature.

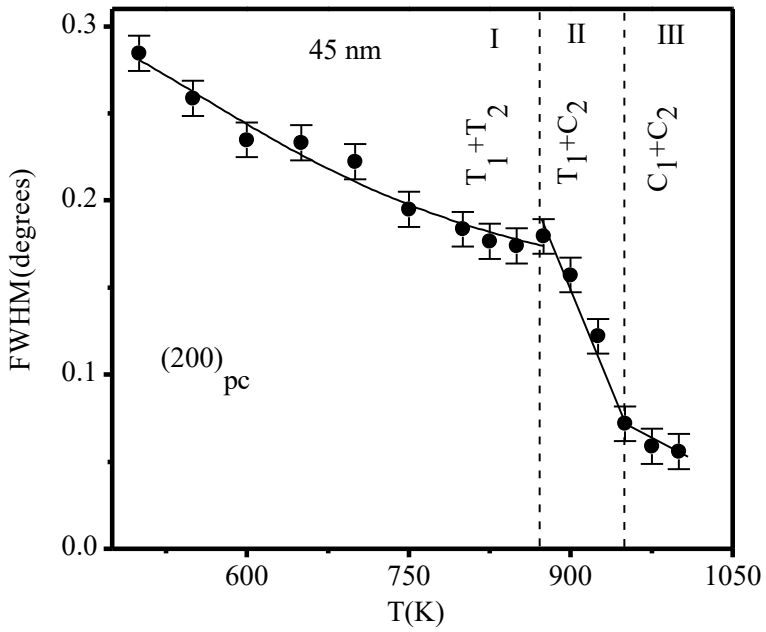

Fig. 7.8 The variation of FWHM of the (200)pc reflection of 45 nm size of BF-0.5PT powder with temperature.

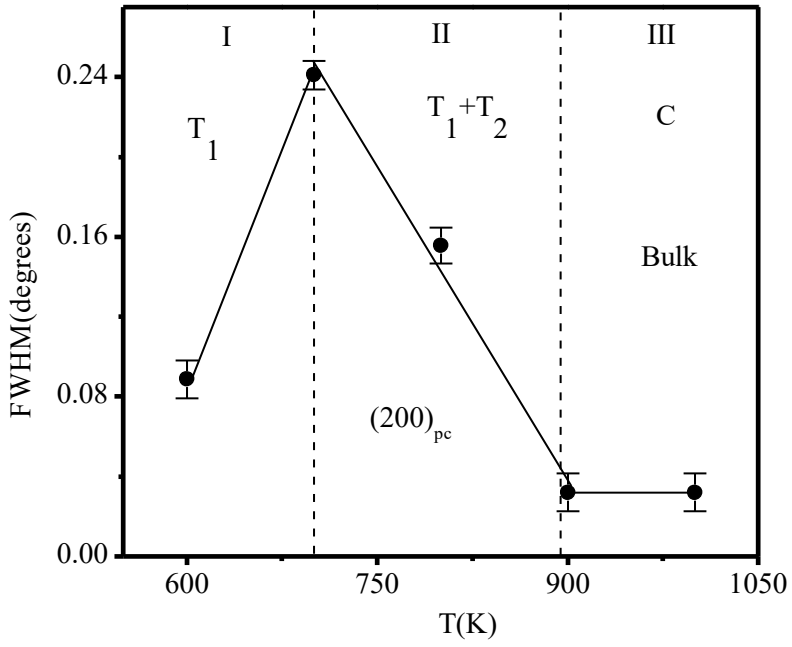

Fig. 7.9 The variation of FWHM of the (200)pc reflection of 45 nm size of BF-0.5PT powder with temperature.

On the other hand in bulk BF0.5PT, the FWHM of (200)pc peak remain constant in third part of fig.7.9. This indicates that tetragonal phase has transformed in single cubic phase at ~ 900K. From above discussion, it is evident that transitions are nearly at same temperature as per the SXRD data.

7.3.3 Variation of structural parameter with size

The variations of lattice parameters with temperature for different sizes are shown in fig 7.10 to fig. 7.12. It is interesting to note that the tetragonality (c/a-1) of T_1 phase decreases from 7.9% at room temperature to 1.81% at 750K for 31 nm of powder.

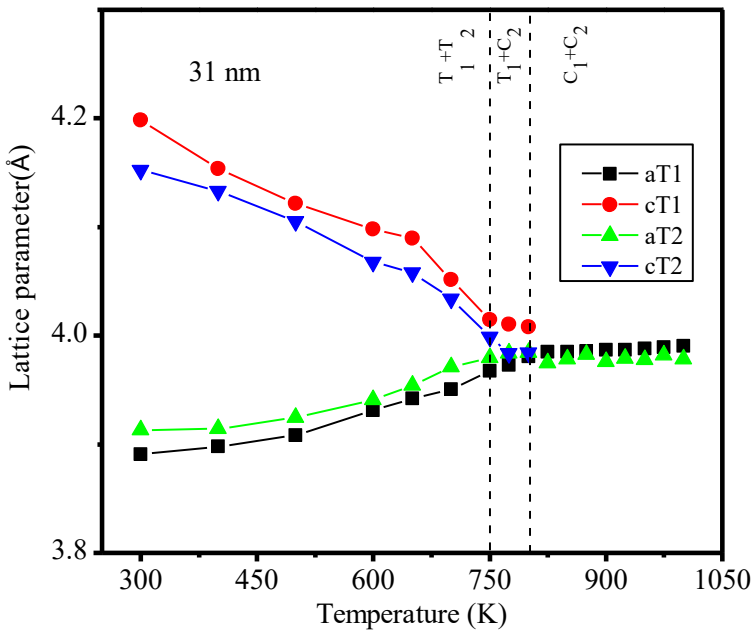

Fig. 7.10 The variation of lattice parameters of tetragonal (T1 and T2) and cubic (C) phases with temperature obtained from LeBail refinement of 31 nm BF-0.5PT powder.

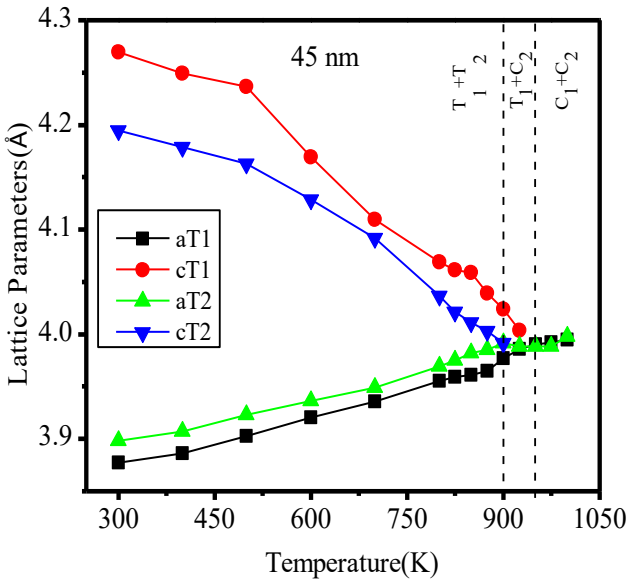

Fig. 7.11 The variation of lattice parameters of tetragonal (T1 and T2) and cubic (C) phases with temperature obtained from LeBail refinement of 45 nm BF-0.5PT powder.

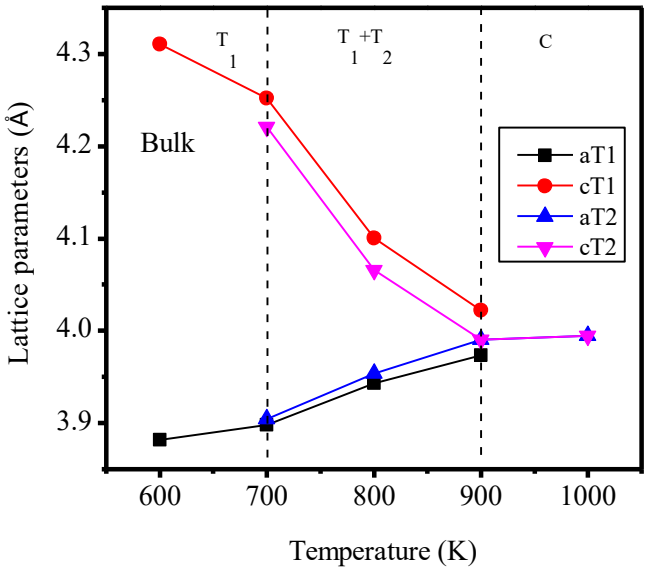

Fig. 7.12 The variation of lattice parameters of tetragonal (T1 and T2) and cubic (C) phases with temperature obtained from LeBail refinement of bulk BF-0.5PT powder.

The magnitude of tetragonality of this size still large as compared to tetragonality observed for even pure $PbTiO_3$ (~ 6%) at room temperature. On the other hand, though the tetragonality of T_2 phase is nearly 1.81% at 750K which increases to ~ 6.12% on cooling down to 300K. Similar kind of phenomena is also observed for 45 nm powder of BF-0.5PT, where tetragonality decreases from ~10.1% at 300K to ~1.87% at 875K. These results shows that how sizes are affect the tetragonality of powder samples. The bulk powder shows ~11.06% tetragonality at 600K which is much larger value that of pure $PbTiO_3$ powder at room temperature.

7.4 Summary and conclusions

The main conclusions of this chapter may summarize as under:

(1) The tetragonal to tetragonal phase transition in BF-0.5PT, i.e an isostructural phase transition is observed by preserving the both space group symmetry.

(2) The ferroelectric transition temperature decreases with size in BF-0.5PT. The 31 nm and 45 nm powder shows their ferroelectric transition around 800 K and 950K respectively, while for the bulk powder it is in between 950K to 1000K.